Tightly Coupling GPS with Lane Markings for Autonomous Vehicle Navigation

Zui Tao, Philippe Bonnifait

Tightly Coupling GPS with Lane Markings for Autonomous Vehicle Navigation

Zui Tao[1,2], Philippe Bonnifait[1,2]

***Abstract*— Tightly coupling GPS pseudorange and Doppler measurements with other sensors is a way to increase accuracy and integrity of the positioning information particularly when it is computed autonomously. Highly accurate digital maps are also more and more key components for autonomous vehicle navigation and can enhance the localization system. In this paper, a video camera is used to get relative information with respect to lane markings and dead-reckoning sensors are also integrated to provide positioning information with high availability. A reduced order state space modeling of the observation problem is proposed in order to get an efficient real-time computing system. Thanks to an adequate error model of the GPS pseudoranges and a measured input state space formalization, a Kalman filter with correlated noises is developed. Experimental results show that this tightly coupled approach clearly improves the performance in terms of accuracy and integrity compared to a loosely coupled method that uses GPS fixes computed by an external receiver.**

I. Introduction

Recently, impressive demonstrations of self-driving cars using production-based sensors and enhanced maps have been made on both rural and urban routes [1][2][3]. In most cases, an on-road assumption and the use of an informative digital map make it possible to realize low-cost autonomous driving. In the research community of Intelligent Transportation Systems, generation of detailed digital maps has done significant progress [4][5] to the point that map-aided perception [6] and localization are now intensively considered for autonomous navigation.

Global Navigation Satellite Systems are widely used in vehicle navigation applications. When integrating GPS with other sources of information, there are two main kinds of approaches: a loosely coupled approach which uses directly the GPS fix and a tightly coupled one which uses the GPS observables like pseudoranges, Dopplers and carrier phase measures. Loosely coupled methods have to estimate biases on the GPS fixes to improve the fusion process. The bias error is typically due to atmospheric effects and can be hardly observed by a stand-alone GPS loosely coupled with dead-reckoning (DR) sensors. In [7], the GPS bias is estimated using the perception of lanes and crosswalks stored in the map data. In [8], different GPS bias models are proposed and compared. However, loosely coupled methods depend on the GPS receiver and are behind its software processing which is particularly difficult to model. In this paper, we thus propose to estimate the bias on every pseudorange.

The benefits of using a map in tight coupling has been proved for a long time. In [9], a Road Reduction filter is developed to calculate pseudorange corrections derived from the digital road network. Since no perception information is required, this macro-scale approach introduces a map pseudo-measurement by projecting the GPS fix onto the road center-line. A navigation system incorporating this approach can achieve an horizontal position accuracy of 10m (1σ) typically [10]. An alternative is to use the map as a heading sensor by considering that the map precision is often better than its accuracy [11]. In order to benefit from a highly accurate map as described in [4] and to remove non-zero mean errors introduced by map matching on poly-lines, a vehicle needs to measure its relative position w.r.t. the lane in which it is traveling by integrating a perception information such as lane marking detections. With this objective in mind, this paper proposes a tightly coupled approach that integrates a camera observations and a lane marking map similar to the one used in [12] by using an extended Kalman filter with correlated noises (EKF-CN). Recent results on tightly coupling can be found in [13][14].

Loosely coupled methods as the one proposed in [12] can improve the lateral localization accuracy up to a decimeter-level. The longitudinal error is also controlled thanks to the heading variation of the trajectory. In the tightly coupling case, the longitudinal uncertainty can be further corrected by the pseudoranges whose line-of-sight directions are along the driving direction as shown in [15].

Important performance metrics are not limited to accuracy. Integrity is also crucial for autonomous vehicles. The integrity risk is defined as probability that the position error exceeds predefined alert limits. In this paper, the integrity risk of the estimated position is set to 10^{-2} (1%). By ignoring the faults of the sensors and by assuming that the noises follow Gaussian distributions, the corresponding bound of the estimated position is $\pm 2.58\sigma$. Therefore, an integrity failure happens when the estimated horizontal positioning error (HPE) is beyond this bound centered on the estimate. As discussed in [16], Bayesian state filtering is often over-confident, and so we are interested in studying here this issue and comparing the integrity performance of both loosely and tightly coupled methods.

The remainder is organized as follows. Section II introduces the system modeling and reminds the lane marking aided vehicle localization. Section III introduces the GPS measurement models and a reduced-order Kalman filtering is proposed for efficient embedded computation. Results of outdoor experiments are presented and analyzed in section IV. Conclusions on the proposed tightly coupled method compared to a loosely coupled one are given in section V.

The authors are with [1]*Université de Technologie de Compiègne (UTC)*, [2]*CNRS Heudiasyc UMR* 7253.

II. Lane marking localization

If the vehicle approximately knows where it is located in the map, it is possible to implement a lane marking localization method that corrects DR estimates based for instance on wheel odometry. We explain in this section the key concepts to implement such an approach.

A. Frames

A local navigation frame R_O tangent to the Earth is defined to have its x axis pointing to the East, y to the North and z oriented upwards w.r.t. the WGS84 ellipsoid (Fig. 1a). By choosing the origin O close to the navigation area, the vehicle trajectory is locally planar. Two more frames have to be defined. In Fig. 1b, R_M denotes the mobile vehicle body frame with its longitudinal axis x_M pointing forward and its lateral axis y_M pointing left hand. The camera frame R_C is located at the front of the vehicle even if the camera is located behind the windscreen with a position offset (C_x, C_y) in R_M. P_x is the translation from point M up to the bumper. In the following, the coordinates are expressed by default in R_O.

B. Dead-reckoning

The linear velocity of each rear wheel is measured by the ABS speed sensors. The linear velocity is calculated by $v^m = (v^m_{rl} + v^m_{rr})/2$, where v^m_{rl} and v^m_{rr} denote the measured linear velocity of the left and right rear wheels respectively.

The angular velocity of the vehicle (ω^m) is measured by the ESP yaw rate gyro. An estimate of the pose of the vehicle is provided by integrating these measurements from an initial known pose.

Please note that the measurements are affected by noise ($v^m = v + \gamma^v$; $\omega^m = \omega + \gamma^\omega$) and so the dead-reckoned estimate drifts with respect to the traveled distance.

C. Lane marking map

The lane marking map used in this paper mainly consists of two-lane roadways with dashed lane markings in the center of the road and solid lane markings on the both sides of the road. Lane markings are expressed by polylines. The map is expressed in R_O and reaches a centimeter-level accuracy.

D. Camera measurement

Let L denote the lane marking detection located at ordinate C_0 in R_C (see Fig. 1b). Its coordinates in R_O are given by (x, y being the position and θ the heading angle):

$$\begin{bmatrix} x_L \\ y_L \end{bmatrix} = \begin{bmatrix} P_x \cdot \cos\theta + C_0 \cdot \sin\theta + x \\ P_x \cdot \sin\theta - C_0 \cdot \cos\theta + y \end{bmatrix} \quad (1)$$

In Fig. 1b, $[AB]$ represents the detected lane marking segment. The coordinates of point A and B are (x_A, y_A) and (x_B, y_B) in R_O. Let us define a vector $V = (x_{AB}, y_{AB})^T$ with $x_{AB} = x_B - x_A$ and $y_{AB} = y_B - y_A$. Point L on segment $[AB]$ meets:

$$\begin{cases} x_L = x_A + \lambda \cdot x_{AB} \\ y_L = y_A + \lambda \cdot y_{AB} \end{cases} \quad (2)$$

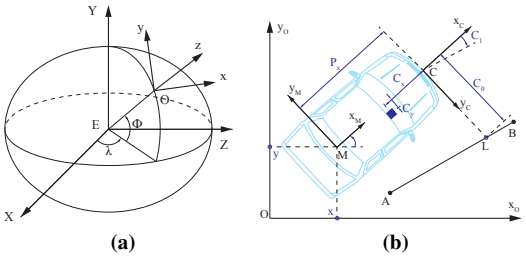

Fig. 1: *Frames*

with $\lambda \in [0, 1]$. Plugging Eq. (1) into Eq. (2), we have:

$$\begin{cases} P_x \cdot \cos\theta + C_0 \cdot \sin\theta + x = x_A + \lambda \cdot x_{AB} \\ P_x \cdot \sin\theta - C_0 \cdot \cos\theta + y = y_A + \lambda \cdot y_{AB} \end{cases} \quad (3)$$

Because $x_{AB} \cdot cos\theta + y_{AB} \cdot sin\theta \neq 0$ (the detected segment is not perpendicular to the vehicle), the camera observation model is derived by Eq. (3) as:

$$C_0 = \frac{(P_x \cdot \sin\theta + y - y_A)\, x_{AB} - (P_x \cdot \cos\theta + x - x_A)\, y_{AB}}{x_{AB} \cdot cos\theta + y_{AB} \cdot sin\theta} + \beta_c \quad (4)$$

where β_c is the measurement noise.

E. Map-matching

Map-matching consists to determine which is the lane marking segment $[AB]$ that the camera has detected. In this paper, the marking type (e.g. dashed or solid) given by the video camera is used to map-match the detected lane marking segment. In a first stage, a set S of candidate segments is selected based on the following conditions:

- The lane marking type is consistent with the one estimated by the camera;
- The orientation of the segment is close to the heading of the vehicle;
- The distance $dist$ between point L and the candidate segment is less than the width of the road.

In a second stage, the segment s which has the minimal dist is chosen as the map-matching result:

$$\text{Map\_matched\_segment} = \arg \min_{s \in \{S\}} \{\text{dist}\} \quad (5)$$

III. Tightly coupling GPS

In this section, we present a strategy for tightly coupling the GPS raw measurements with the lane marking localization.

A. GPS measurements

The GPS raw measurements considered here are $L1$ pseudoranges and Dopplers on the visible satellites.

The position of the GPS antenna with respect to the body frame is taken into account.

$$\begin{cases} x_a = x + cos\theta \cdot t_x - sin\theta \cdot t_y \\ y_a = y + sin\theta \cdot t_x + cos\theta \cdot t_y \\ z_a = z + t_z \end{cases} \quad (6)$$

Where $[x, y, z]^T$ is the 3D position of the vehicle, $[t_x, t_y, t_z]^T$ is the position of the receiver antenna in R_M

and $X_a = [x_a, y_a, z_a]^T$ is the position of the receiver antenna in R_O.

For a given satellite i, its position vector $X_s^i = \left[x^i, y^i, z^i\right]^T$ is reconstructed from the received navigation message (GPS data). The corresponding pseudorange is:

$$\rho^i = R^i + c \cdot dt_u - c \cdot dt_s + \delta_{TGD} + \delta_{rel} + \delta_{iono} + \delta_{tropo} \quad (7)$$

with R^i being the geometrical distance between the observed satellite and the receiver antenna $\left(R^i = \left\|X_a - X_s^i\right\|\right)$, $c \cdot dt_u$ the range equivalent of the receiver clock offset, $c \cdot dt_s$ the range equivalent of the satellite clock offset, δ_{TGD} the timing Group Delay, δ_{rel} the range equivalent of the relativity effect on the satellite clock, δ_{iono} the ionospheric delay and δ_{tropo} the tropospheric delay.

For every satellite, the GPS receiver gets also, in its ephemeris data, some information to compute estimates of dt_s, δ_{TGD} and δ_{rel}. It can also estimate δ_{iono} and δ_{tropo} by using classical atmosphere models implemented in open source software like [17]. By correcting the pseudorange with these estimated parameters, equation 7 becomes:

$$\rho^i = R^i + c \cdot dt_u + \varepsilon_{pr}^i + \beta^i \quad (8)$$

where ε_{pr} represents the residual (non-white) errors of the pseudorange. β^i is the measurement noise. c is the speed of light.

The Doppler shift is caused by the relative motion between the satellite and the receiver antenna. By defining the line-of-sight vector u_{los}^i of satellite i as,

$$u_{los}^i = \left(X_a - X_s^i\right) / R^i \quad (9)$$

the Doppler shift is measured and linked to the GPS antenna trough the following equation [18]:

$$\dot{\rho}^i = \left(V_r - V_s^i\right) \bullet u_{los}^i + c\dot{\delta t}_u + \beta_d^i \quad (10)$$

Where $V_r = [\dot{x}, \dot{y}, \dot{z}]^T$ is the velocity of the receiver and $V_s^i = \left[\dot{x^i}, \dot{y^i}, \dot{z^i}\right]^T$ is the one of satellite i. $\bullet$ denotes the dot product. β_d^i is the measurement noise.

For a numerically good computation, the filter estimates ranges equivalent values of the receiver clock parameters:

$$d = c \cdot dt_u \quad \dot{d} = c \cdot \dot{dt}_u$$

B. System modeling

Let us look for a planar model of the system in order to have an efficient state observer in terms of computations with a limited number of sensors. The localization problem can be reduced to 2D by considering z^a as constant during the current navigation stage. The main sources of range error are (see Fig. 2):

- Pseudoranges residuals errors ε_{pr};
- Inaccurate satellite position estimates due to the use of real-time navigation messages ε_{Sat};
- The fact that the evolution area is not exactly planar ε_z.

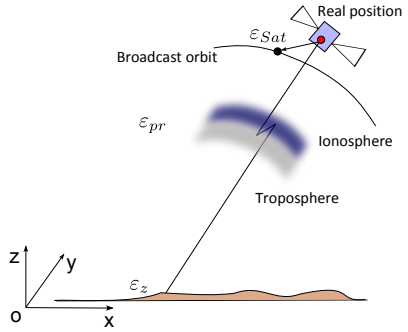

Fig. 2: *Range-error sources*

We propose to estimate a range-error parameter ε that results from the combination of ε_{Sat}, ε_{pr} and ε_z. A first order auto-regressive shaping filter is used by (the subscript k being the time stamp):

$$\varepsilon_k^i = a \cdot \varepsilon_{k-1}^i + \alpha_{k-1}^{\varepsilon} \quad (11)$$

Where α^{ε} is the driving noise.

Let us consider a front-wheel drive vehicle with the assumption of a slip-free motion of the rear wheels. The speed vector is therefore collinear to x_M.

With n satellites in view, the state vector X becomes:

$$X = \left[x, y, \theta, b, d, \dot{d}, \varepsilon^1, \ \cdots \ , \varepsilon^n\right]^T \quad (12)$$

Where b is the bias of the gyro.

With a 2D unicycle kinematic model, the evolution model is given by:

$$\widehat{X}_k = f\left(\widehat{X}_{k-1}, U_k^m, \alpha_k\right) \Leftrightarrow \begin{cases} x_k = x_{k-1} + T \cdot v_k^m \cdot cos\theta_{k-1} \\ y_k = y_{k-1} + T \cdot v_k^m \cdot sin\theta_{k-1} \\ \theta_k = \theta_{k-1} + T \cdot (w_k^m - b_{k-1}) \\ b_k = b_{k-1} + \alpha_k^b \\ d_k = d_{k-1} + T \cdot \dot{d}_{k-1} + \alpha_k^d \\ \dot{d}_k = \dot{d}_{k-1} + \alpha_k^{\dot{d}} \\ \varepsilon_k^1 = a \cdot \varepsilon_{k-1}^1 + \alpha_k^{\varepsilon 1} \\ \vdots \\ \varepsilon_k^n = a \cdot \varepsilon_{k-1}^n + \alpha_k^{\varepsilon n} \end{cases} \quad (13)$$

Where $U^m = [v^m, \omega^m]^T$ denotes the measured input vector and T the sampling period. A random constant model has been considered to handle the bias b.

The wheel speed sensor measurement noise v_v and the gyro measurement noise v_ω are supposed to be zero-mean independent white noises. N denotes their covariance matrix. The covariance of the model noise $\alpha_k = \left[\begin{array}{ccccccc} \alpha_k^b & \alpha_k^d & \alpha_k^{\dot{d}} & \alpha_k^{\varepsilon 1} & \ldots & \alpha_k^{\varepsilon n} \end{array}\right]^T$ of equation (13) is denoted by Q.

C. GPS measurement validation

At time instant k, when the GPS measurements are available, a validation step is performed on the measurements of every satellite to avoid the use of badly tracked satellites and to reject multipath.

For a Doppler measurement, the validation process is:

- C/N_0 gating: Check that C/N_0 is high enough (e.g. 38 dBHz).

- Elevation mask: The elevation angle of satellite i is calculated using X_s^i and the current estimate $\widehat{X}_{k|k-1}$. The elevation mask angle is usually set to 15 degrees.
- Innovation gating: Check the Normalized Innovation Squared [19].

A Doppler is in general more reliable than a pseudorange. Therefore, a pseudorange can be used only when its corresponding Doppler measurement is valid. For every pseudorange, its innovation η_i is computed and used to validate or reject the measurement.

By denoting $A_k = \frac{\partial f\left(\widehat{X}_{k-1|k-1}, U_k^m\right)}{\partial X}$, $B_k = \frac{\partial f\left(\hat{X}_{k-1|k-1}, U_k^m\right)}{\partial U^m}$, the tightly coupling solver is described by Algorithm 1 in which the Dopplers are used at first. Additionally a Mahalanobis distance threshold is set to reject the mismatch before using C_0 to update the state vector. The process is time-triggered with the CAN bus data which has the highest rate. The latencies of the GPS and camera measurements are, in the current implementation, neglected. Since the camera provides essentially lateral corrections, neglecting its latency has almost no impact on the accuracy.

Algorithm 1 An iteration stage of the method

In out: $\widehat{X}$, P //estimated state and covariance matrix

$U^m = [v^m, \omega^m]^T$ =**Get**(DR measurements)
$\widehat{X} = f\left(\widehat{X}, U^m\right)$
$P = A_k \cdot P \cdot A_k^T + B_k \cdot N \cdot B_k^T + Q$
if New GPS data is available **then**
  $\left[\rho^{1,\cdots,n}, \dot{\rho}^{1,\cdots n}\right]$ =**Get**(GPS measurements)
  Good_Doppler=$\varnothing$ Good_Pr=$\varnothing$
  for $j = 1, \ldots, n$ **do**
    if ($\dot{\rho}^j$ is valid) **then** // Please refer to Section III-C
      Add($\dot{\rho}^j$) to the Good_Doppler list
    end if
  end for
  $\left[\widehat{X}, P\right]$ =**Update**($\widehat{X}$,P,Good_Doppler)
  for $j = 1, \ldots, n$ **do**
    if ($\dot{\rho}^j$ is valid)&(η_i < Threshold) **then**
      Add(ρ^j) to the Good_Pr list
    end if
  end for
  $\left[\widehat{X}, P\right]$ = **Update**($\widehat{X}$,P,Good_Pr)
end if
if New camera measurements are available **then**
  $[C_{0,k}, laneType]$ =**Get**(camera measurements)
  $[AB]$=**Map_match**$\left(\widehat{X}, C_{0,k}, laneType, map\right)$
  if ($[AB]$ is consistent with the vehicle state) **then**
    $\left[\widehat{X}, P\right]$ = **Update**$\left(\widehat{X}, P, C_{0,k}, [AB]\right)$
  end if
end if

One can note that the filter uses a measured linear velocity v^m in the Doppler observation model (Eq. 10). Therefore, the estimation process has correlated noises. Please refer to [20] for more details about the EKF-CN equations.

Model noises variances	Measurement noises variances
$Var\left(\alpha^b\right) = 5 \times 10^{-10}$	$Var\left(\beta_c\right) = 0.16$
$Var\left(\alpha^d\right) = 1 \times 10^{-3}$	$Var\left(\beta\right) = S \cdot 10^{\frac{-C/N_0^i}{10}}$
$Var\left(\alpha^{\dot{d}}\right) = 1 \times 10^{-4}$	$Var\left(\beta_d\right) = 0.05$
$Var\left(\alpha^{\varepsilon}\right) = 1 \times 10^{-4}$	$Var\left(\gamma^v\right) = 1 \times 10^{-4}$
	$Var\left(\gamma^{\omega}\right) = 2.5 \times 10^{-3}$

TABLE I: *Tuned EKF-CN parameters (International System Units)*

IV. Experimental results

Outdoor experiments have been carried out near Paris France in May 2013. Three tests were performed on the same road, in urban conditions, with an automotive experimental vehicle. Test 1 and Test 2 were conducted in the morning and test 3 in the afternoon. During the test, the vehicle passed in a strong urban canyon of 300 meters with satellites outages and multipaths. The traveling distance of every test was about 2km with a typical speed of 30 km/h in the straight lines. The experimental vehicle was equipped with an IMU Oxford RT3000 which provided ground truth data at 100Hz rate. A CAN-bus gateway was used to access to the wheel speed sensors and to the yaw rate gyro. The measured input $[v^m, w^m]^T$ from the CAN bus were available at 100Hz. A Mobileye camera was used to detect the lane markings at 10Hz. A low-cost U-blox 6T GPS receiver with a patch antenna providing pseudoranges and Dopplers measurements at 5Hz was used.

The measurement noise β^i in Eq. (8) is supposed to be white and zero mean. As it is not stationary as indicated in [21], its variance σ_i^2 is modeled by a Wieser's model in which the measured carrier-to-noise density ratio C/N_0 is used as a quality indicator:

$$\sigma_i^2 = S \cdot 10^{\frac{-C/N_0^i}{10}} \tag{14}$$

Where $S = 60000 m^2 Hz$. Table I specifies every model and measurement noise.

10 satellites were in view during the different tests. The GPS satellite visibility was sometimes very constrained due to the urban canyon and due to buildings near the test area.

Localization performance can be studied in terms of longitudinal and lateral performances. Fig. 3 shows the lateral and longitudinal positioning errors of test 2 for loosely and tightly coupling. After t = 350s, the vehicle is back to the parking lot where lane markings are not stored in the map and so the localization system is not map-aided in this area.

The bias on every pseudorange is initialized to zero. For each subplot of Fig. 4, the abscissa expresses time on seconds, the ordinate gives every estimated bias ε^i on meters. Satellites 4 and 13 are under the elevation mask ($15°$) and so their measurements are not used in the localization solver. Moreover, the measurements of satellite 26 became available only after 100s and were lost after 200s. The estimated biases are quite smooth, in the order of few meters and stay bounded during all the trial.

Table II gives performance metrics for both the loosely coupled solver (LC) proposed in [12] and the tightly coupled

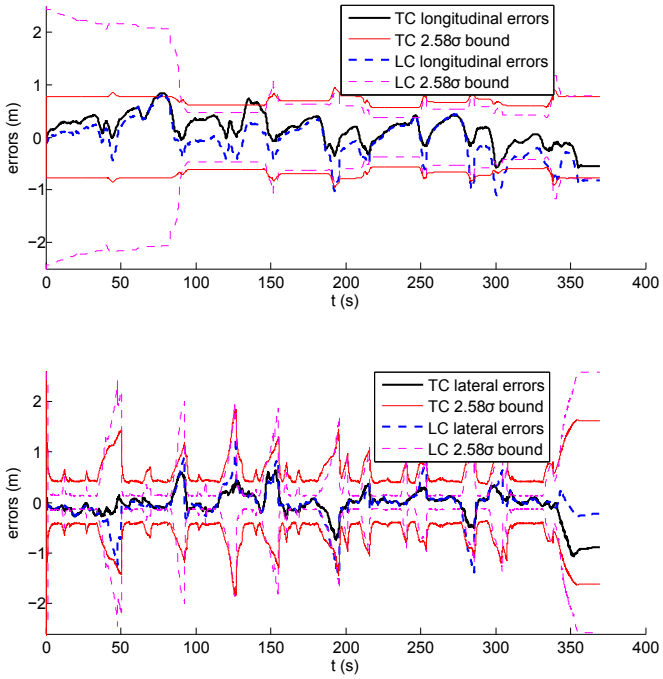

Fig. 3: *Longitudinal/lateral positioning errors. TC: tightly coupling; LC: loosely coupling*

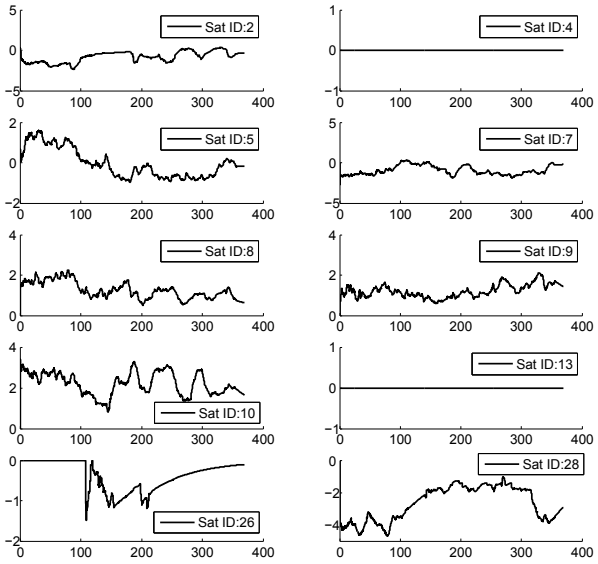

Fig. 4: *Estimated bias on pseudoranges*

solver (TC) proposed in this paper.

Fig. 5 shows the cumulative distribution of horizontal positioning errors of the three tests by four methods: stand-alone GPS, loosely coupling DR/GPS/Map, tightly coupling DR/GPS and tightly coupling DR/GPS/Map. It is noticeable that tightly coupling GPS with DR improves the accuracy compared with stand-alone GPS. The accuracy of the tightly coupled method is further improved by integrating the lane marking map. The $95th$ percentiles of the four methods are respectively 0.88m, 1.54m, 2.12m and 4.64m. 96.8% of the tightly coupling result reaches sub-meter accuracy.

The loosely coupled method relies on the GPS fixes computed by stand-alone GPS receiver. When the GPS receiver suffers from big errors during a long time, the

		Test 1	Test 2	Test 3	Global
Std. dev. (m^2)	LC	0.46	0.31	0.93	0.62
	TC	0.25	0.24	0.28	0.26
Max (m)	LC	2.67	1.62	5.29	5.29
	TC	1.59	1.11	1.63	1.63
Median (m)	LC	0.36	0.33	0.33	0.34
	TC	0.31	0.33	0.32	0.32
95th percentile (m)	LC	1.56	1.02	3.06	1.54
	TC	0.87	1.03	0.90	0.88
Integrity failure rate	LC	22.8%	13.3%	31.6%	22.1%
	TC	3.9%	4.6%	15.1%	7.6%

TABLE II: *Horizontal positioning error statistics*

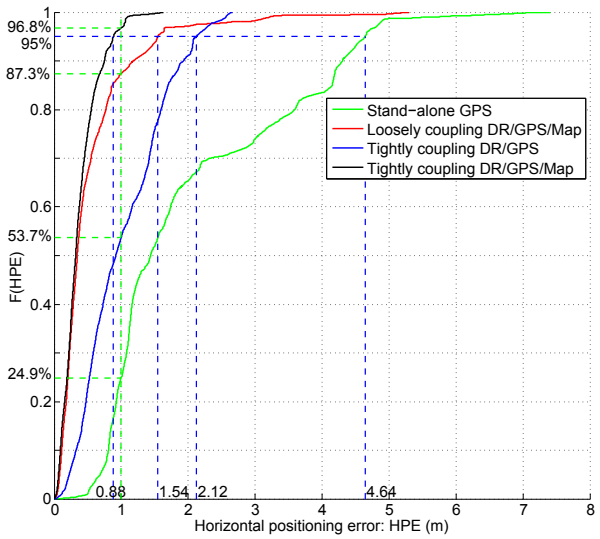

Fig. 5: *Cumulative distribution function (CDF) of the HPE for the different methods*

loosely coupled solver is not able to estimate the biases efficiently. Although the $95th$ percentile is 1.54m, the biggest error reaches 5.29m.

Fig. 6a shows the global integrity performance of the loosely and tightly coupled methods. The gray area corresponds to the overconfident occasions of the filters. The global failure rate of the loosely coupled method is about 22% (Table II). The tightly coupled method reduces the integrity failure rate to 7.6% which is the same order as the predefined integrity risk of 1% even if it is a bit higher. The tightly coupled method is therefore more reliable. Now let us evaluate the precision of the results by considering the distribution of the estimated 2.58σ bound. Fig. 7 shows the tightly coupled method provides confidence domains that are smaller than 1.26m during 95% of the time which is a good improvement compared to the 2.06m of the loosely coupled one. As confidence is in practice compared to a threshold to indicate "use" or "don't use" to the client application, it is important, in terms of availability of the positioning information, to provide as small as possible confidence zones. To resume this integrity analysis, one can notice the confidence domains computed by the tightly coupled approach are smaller than the ones of the loosely coupled approach and they are more reliable in the sense that the

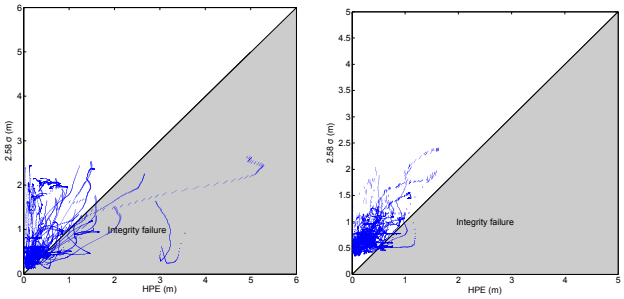

(a) *Loosely coupled method* **(b)** *Tightly coupled method*

Fig. 6: *Integrity plot*

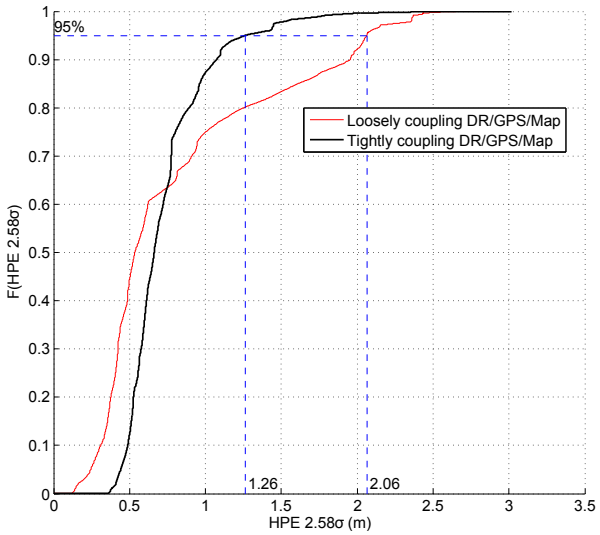

Fig. 7: *CDF of the estimated confidence domain of HPE*

ground truth is more often included in the confidence zone.

V. Conclusion

In this paper, we have proposed and studied a method to merge raw GPS measurements and lane marking measurements. In order to reduce the dimension of the state vector, the linear and angular velocity are used as measured input. The vehicle is also assumed to travel on a flat surface thanks to the use of a navigation frame close to the navigation area. An error model has been proposed to estimate the errors on GPS pseudoranges. A tightly coupled EKF-CN solver has been developed to reduce the calculation and improve the real-time performance. For testing the approach, DR sensors from the ABS and ESP systems, a L1-GPS receiver and the lane marking measurements from the lane departing warning system of the experimental vehicle have been used. Outdoor experiments have been carried out to compare the loosely coupled and tightly coupled methods. The tightly coupled method gives a better accuracy and a better reliability. This system provides a very cost-effective solution for the localization task of autonomous vehicles.

Acknowledgments

The authors would like to thank Javier-Ibañez Guzman, Nabil Chaari and Stéphane Bonnet for their support in the experiments.

References

[1] J. Ziegler *et al.*, "Making bertha drive an autonomous journey on a historic route," *Intelligent Transportation Systems Magazine, IEEE*, vol. 6, no. 2, pp. 8–20, Summer 2014.

[2] P. Furgale *et al.*, "Toward automated driving in cities using close-to-market sensors: An overview of the v-charge project," in *Intelligent Vehicles Symposium (IV), 2013 IEEE*, June 2013, pp. 809–816.

[3] M. Schreiber, C. Knoppel, and U. Franke, "Laneloc: Lane marking based localization using highly accurate maps," in *Intelligent Vehicles Symposium (IV), 2013 IEEE*, June 2013, pp. 449–454.

[4] D. Betaille and R. Toledo-Moreo, "Creating enhanced maps for lane-level vehicle navigation," *Intelligent Transportation Systems, IEEE Transactions on*, vol. 11, no. 4, pp. 786–798, Dec 2010.

[5] S. Brummer, F. Janda, G. Maier, and A. Schindler, "Evaluation of a mapping strategy based on smooth arc splines for different road types," in *Intelligent Transportation Systems - (ITSC), 2013 16th International IEEE Conference on*, Oct 2013, pp. 160–165.

[6] M. Kurdej, J. Moras, V. Cherfaoui, and P. Bonnifait, "Controlling remanence in evidential grids using geodata for dynamic scene perception," *International Journal of Approximate Reasoning*, vol. 55, no. 1, pp. 355–375, January 2014.

[7] K. Jo, K. Chu, and M. Sunwoo, "Gps-bias correction for precise localization of autonomous vehicles," in *Intelligent Vehicles Symposium (IV), 2013 IEEE*, June 2013, pp. 636–641.

[8] Z. Tao, P. Bonnifait, V. Fremont, and J. Ibanez-Guzman, "Mapping and localization using gps, lane markings and proprioceptive sensors," in *Int. Robots and Systems, 2013 IEEE/RSJ International Conf. on*, Nov 2013, pp. 406–412.

[9] G. Taylor, G. Blewitt, D. Steup, S. Corbett, and A. Car, "Road reduction filtering for gps-gis navigation," *Transactions in GIS*, vol. 5, no. 3, pp. 193–207, 2001.

[10] P. Groves, *Principles of GNSS, inertial, and multi-sensor integrated navigation systems*, ser. GNSS technology and applications series. Artech House, 2008.

[11] C. Fouque and P. Bonnifait, "On the use of 2d navigable maps for enhancing ground vehicle localization," in *Int. Robots and Systems, 2009. IEEE/RSJ International Conf. on*, Oct 2009, pp. 1885–1890.

[12] Z. Tao, P. Bonnifait, V. Fremont, and J. Ibanez-Guzman, "Lane marking aided vehicle localization," in *Int. Transp. Systems, 2013 16th International IEEE Conf. on*, Oct 2013, pp. 1509–1515.

[13] A. Rabaoui, N. Viandier, E. Duflos, J. Marais, and P. Vanheeghe, "Dirichlet process mixtures for density estimation in dynamic nonlinear modeling: Application to gps positioning in urban canyons," *Signal Processing, IEEE Transactions on*, vol. 60, no. 4, pp. 1638–1655, April 2012.

[14] U. Iqbal *et al.*, "Pseudoranges error correction in partial gps outages for a nonlinear tightly coupled integrated system," *Int. Transp. Systems, IEEE Transactions on*, vol. 14, no. 3, pp. 1510–1525, Sept 2013.

[15] A. Vu, A. Ramanandan, A. Chen, J. Farrell, and M. Barth, "Real-time computer vision/dgps-aided inertial navigation system for lane-level vehicle navigation," *Int. Transp. Systems, IEEE Transactions on*, vol. 13, no. 2, pp. 899–913, June 2012.

[16] V. Drevelle and P. Bonnifait, "Localization confidence domains via set inversion on short-term trajectory," *Robotics, IEEE Transactions on*, vol. 29, no. 5, pp. 1244–1256, Oct 2013.

[17] R. Harris and R. Mach, "The gpstk: an open source gps toolkit," *GPS Solutions*, vol. 11, no. 2, pp. 145–150, 2007.

[18] C. Fouque and P. Bonnifait, "Matching raw gps measurements on a navigable map without computing a global position," *Int. Transp. Systems, IEEE Transactions on*, vol. 13, no. 2, pp. 887–898, 2012.

[19] C. Fouque, P. Bonnifait, and D. Betaille, "Enhancement of global vehicle localization using navigable road maps and dead-reckoning," in *Position, Location and Navigation Symposium, 2008 IEEE/ION*, May 2008, pp. 1286–1291.

[20] P. Bonnifait, G. Garcia, and F. Peyret, "A system for 3d localization of civil-engineering machines," in *Workshop "Navigation of Outdoor Autonomous Vehicles"*, May 1998.

[21] A. Wieser, M. Gaggl, and H. Hartinger, "Improved positioning accuracy with high-sensitivity gnss receivers and snr aided integrity monitoring of pseudo-range observations," in *Proceedings of the 18th International Technical Meeting of the Satellite Division of The Institute of Navigation (ION GNSS 2005)*, Sept. 2005, pp. 1545–1554.